ACS OMEGA

Open Access

http://pubs.acs.org/journal/acsodf

Article

Exploring ^{99m}Tc-Labeled Iron-Binding Glycoprotein Nanoparticles as a Potential Nanoplatform for Sentinel Lymph Node Imaging: Development, Characterization, and Radiolabeling Studies

Sanjay Kulkarni, Anuj Kumar, Abhijeet Pandey, Soji Soman, Suresh Subramanian,* and Srinivas Mutalik*

Cite This: *ACS Omega* 2024, 9, 42410−42422

Read Online

ACCESS | Metrics & More | Article Recommendations

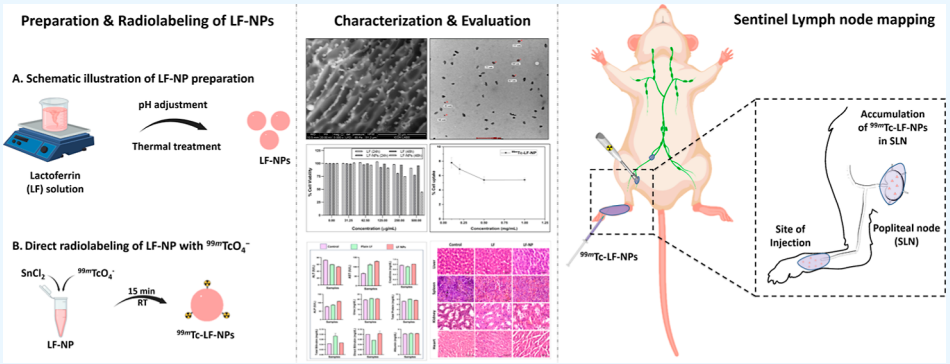

ABSTRACT: Lactoferrin, an iron binding glycoprotein-based nanoparticle, has emerged as a promising platform for drug delivery and imaging. This study presents the potential use of the protein nanocarrier in tracking sentinel lymph nodes for cancer staging. Lactoferrin nanoparticles (LF-NPs) were synthesized using a thermal treatment process and optimized to obtain 60−70 nm particle size with PDI less than 0.2. The NPs were characterized microscopically and spectroscopically, ensuring a comprehensive understanding of their physicochemical properties. The LF-NPs were found to be stable in different pH conditions. Their biocompatibility was confirmed through cytotoxicity assessments on RAW 264.7 cells, and hemolysis assay and in vivo toxicity study reveal their safe profile. Additionally, LF-NPs were successfully radiolabeled with technetium-99m (>90% labeling yield). Cell uptake studies with RAW 264.7 exhibited an uptake of ∼6%. Biodistribution studies in Wistar rats shed light on their in vivo behavior and suitability for targeted drug delivery systems. These findings collectively emphasize the multifaceted utility of LF-NPs, positioning them as a promising platform for diverse biomedical innovations.

1. INTRODUCTION

Early detection of breast cancer is essential for successful treatment, but the potential for cancer to spread to other body parts can make therapy more complicated and affect survival rates. Sentinel lymph nodes (SLNs) are critical in assessing the breast cancer progression. SLN detection and biopsy have become a clinical standard for evaluating involvement of axillary lymph nodes in patients, thereby assisting cancer staging. SLNs are the first nodes receiving lymphatic drainage from the primary tumor site, making them a common route for spreading cancer cells. Tumor cells within SLNs indicate potential metastasis. This influences treatment decisions and prognosis. Traditionally, visual identification using blue dyes and scintigraphic imaging with radioactive technetium-99m (Tc-99m/^{99m}Tc) labeled colloids have been used clinically. In India, ^{99m}Tc-labeled sulfur colloid and human serum albumin (HSA) nanocolloid have been used for SLN detection. However, HSA-based techniques have some drawbacks, including the risk of contamination, immunogenic reactions, and variability in the particle size. Therefore, there is a continued scope for newer research. Several nanoparticle formulations are reported/under development for targeted delivery to SLN.[1,2] Naturally available polymers are always desirable to develop nonimmunogenic and biocompatible nanocarriers.

Lactoferrin (LF), an iron-binding glycoprotein has a molecular weight of 80 kDa and its molecular structure contains two globular lobes stabilized by disulfide bonds.[3] The key role of LF is regulating the free iron concentration in the

Received: June 28, 2024
Revised: August 24, 2024
Accepted: September 13, 2024
Published: October 1, 2024

https://doi.org/10.1021/acsomega.4c05991
ACS Omega 2024, 9, 42410−42422

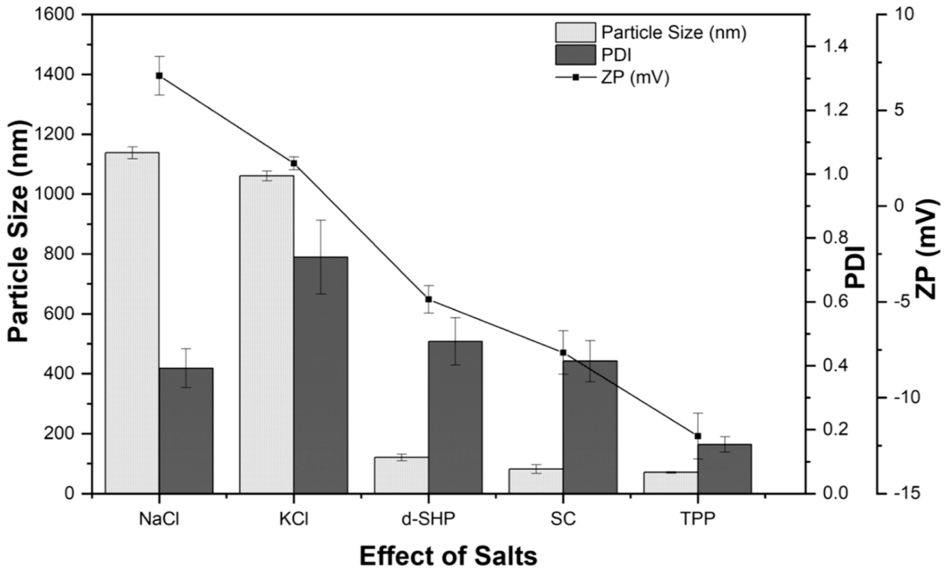

Figure 1. Effect of different salts on particle size, PDI, and zeta potential of LF-NPs.

biological fluids through its ability to bind to the ferric ions (Fe^{3+}), which plays a prominent role in its multifunctional applications like anticancer, anti-inflammatory, immune-stimulating, and antioxidant.[4] Bovine LF is approved by the Food and Drug Administration (USA),[5] Therapeutic Goods Administration (Australia),[6] and the European Food Safety Authority[7] for use in food, sports medicine, and nutritional products. It is commonly used in nutraceutical formulations such as food supplements, infant formulas, and cosmetics.[8] The above factors highlight LF's biocompatibility and usability for in vivo applications. LF's scalability, economic advantage, and ease of surface modification, such as mannosylation and BFCA conjugation, make it a promising candidate to develop radiotracers for SLN imaging. It is expected that SLN radiotracers will be taken up and retained in the primary node with minimal passage further up the lymphatic channel. LF nanoparticles (LF-NPs) are known to bind to membrane receptors on macrophages, facilitating their interaction with lymph node macrophages.[9] This is expected to increase their retention in the SLN, enhancing biological efficacy over conventional SLN radiotracers like the sulfur colloid and HSA nanocolloid.

Tc-99m accounts for >70% of radio-diagnostic scans worldwide.[10] Its advantages include a monoenergetic gamma photon emission with optimal energy (140 keV) for scintigraphic imaging, logistically suitable half-life (6.01 h) for preparing radiolabeled formulation and performing imaging scans, and convenient availability from a Mo-99/Tc-99m column generator by radioactive decay of ^{99} Mo to ^{99m}Tc, which can be selectively eluted in pharmaceutical-grade saline at intervals.[11] The current work deals with the formulation of suitable LF-NPs by temperature-assisted coagulation and detailed characterization, followed by labeling with radioactive isotope Tc-99m and biological evaluation studies to assess its ability to target the SLN.

2. RESULTS AND DISCUSSION

2.1. Preparation of LF-NPs. LF-NPs were prepared using the thermal treatment method in a similar way previously reported by our group.[12] The thermal treatment method offers several advantages over conventional approaches, including considerable reduction in the production stages. It streamlines the procedure and improves scalability. It also reduces the use of toxic chemicals (like alcohols used in denaturation), making it more eco-friendly. The method also controls particle size and morphology, enhancing nanoparticles' functional characteristics and stability.[13] LF-NPs provide notable benefits compared to free LF. Free LF typically has a short half-life, which can reduce its effectiveness. In contrast, LF-NPs can effectively prolong the circulation time of LF because the nanoparticles are better able to evade clearance by the immune system and exhibit greater stability.[14] Various studies have demonstrated that LF-NPs can improve both cytotoxicity and retention of drugs when employed as carriers.[15] In the earlier report, the effect of temperature, pH, and hold time were screened and optimized. However, control over particle size and stability of LF-NPs after lyophilization was a limitation. To address this, we employed different salts as cross-linkers and examined their effect on LF-NP formation (Figure 1). Monovalent salts like sodium chloride (NaCl) and potassium chloride (KCl) led to formation of larger protein particles with sizes more than 500 nm.[16] The divalent salt di-sodium hydrogen phosphate (d-SHP) resulted in the formation of ∼100 nm sized particles but with polydispersity index (PDI) > 0.6.[17] Polyvalent salts like sodium citrate (SC) and TPP yielded a particle size less than 100 nm. However, as the PDI of SC was ∼0.5, TPP, which resulted in PDI < 0.2, was chosen as the final cross-linker. The final optimized parameters were 2.0% w/v protein concentration, with 0.4% w/v TPP heated at 75 °C for 15−20 min. These optimized conditions yielded LF-NPs with particle size 70 ± 5 nm and a PDI of less than 0.2. This improvement by the addition of TPP appears to coincide with the observations in the recent report of Duarte et al.[18]

2.2. Freeze-Drying of LF-NPs. Cryoprotectants of different concentrations were studied to minimize the impact of freeze-drying (Table 1). Of the tested compounds, mannitol and trehalose at suitable concentrations were found to have better cryoprotectant activity. The reconstitution time for both cryoprotectants was <1 min and the reconstituted dispersion appeared as a clear solution. But with dextrose, particle size and PDI increased evidently, and on reconstitution, it appeared slightly hazy with a reconstitution time of 3 min. Trehalose

https://doi.org/10.1021/acsomega.4c05991
ACS Omega 2024, 9, 42410−42422

Table 1. Effect of Cryoprotectants on the Characteristics of the Lyophilized LF-NPs

cryoprotectant	concentration (% w/w)	size (nm)	PDI	reconstitution time (min)
trehalose	5	54.89	0.251	<1
	10	51.56	0.296	<1
	20	**76.32**	**0.18**	**<1**
dextrose	5	241.7	0.364	2
	10	275.3	0.367	3
	20	288.1	0.309	3
mannitol	5	53.4	0.322	<1
	10	85.11	0.415	<1
	20	65.25	0.389	<1
sucrose	5	3277	0.297	3
	10	618.2	0.519	2
	20	245.6	0.320	2

(20% w/w) showing the most narrow size range was selected as the optimal cryoprotectant.

2.3. Characterization of LF-NPs. Fourier transform infrared (FTIR) spectra of the samples exhibited absorption peaks at around 1600 and 1500 cm^{-1}, corresponding to the stretching vibrations of the amide I group (C═O) and amide II groups (N−H). The additional absorption bands of hydroxyl groups and alkyl ether bonds (around 3390 and 1150−1000 cm^{-1}) were present in the freeze-dried products, representing the cryoprotectant. Broadening of peaks in the region 3700−3000 cm^{-1} was observed in the spectra of LF-NPs, corresponding to the hydroxyl and amine groups from thermal induced changes in the structure of LF. Changes in the intensity or shape of these peaks can indicate changes in the presence or accessibility of hydroxyl groups (Figure 2A). Further, differential scanning calorimetry (DSC) thermographs of both LF and LF-NPs exhibited an endothermic peak at 70−80 °C, indicating the denaturation peak of LF. This indicates that the thermal treatment used to prepare the NPs did not induce irreversible structural changes in the protein (Figure 2B). Raman spectra of LF in Figure 2C show the presence of peak at 1000 cm^{-1} (Phe), 1444 cm^{-1} (CH_2), and 1656 cm^{-1} (Amide I).[19] The LF-NP spectra showed the appearance of a sharp peak at 872 cm^{-1}, indicating the presence of trehalose.[20] X-ray diffraction (XRD) diffractograms of LF and LF-NPs are shown in Figure 2D. The presence of noise in the LF diffractogram indicated the amorphous nature of the protein, while the LF-NPs exhibit sharp peaks, indicating the presence of cryoprotectant. LF-NP concentration, as determined by NTA analysis (Figure 3A), was 6.7 × 10^8 particles/mL. The surface morphological attributes of the samples were examined using field emission scanning electron microscopy (FESEM) and transmission electron microscopy (TEM), as shown in Figure 3B,C. The nanoparticles were asymmetrical, and the size range was approximately 60 ± 10 nm.

2.4. Stability of LF-NPs. Figure 3D details the stability of LF-NPs when incubated for 24 h under different pH conditions. It was observed that LF-NPs were stable in the pH range of 4.5−7.4 under both refrigerated conditions and room temperature. The changes in the particle size and PDI with time under different storage conditions were not

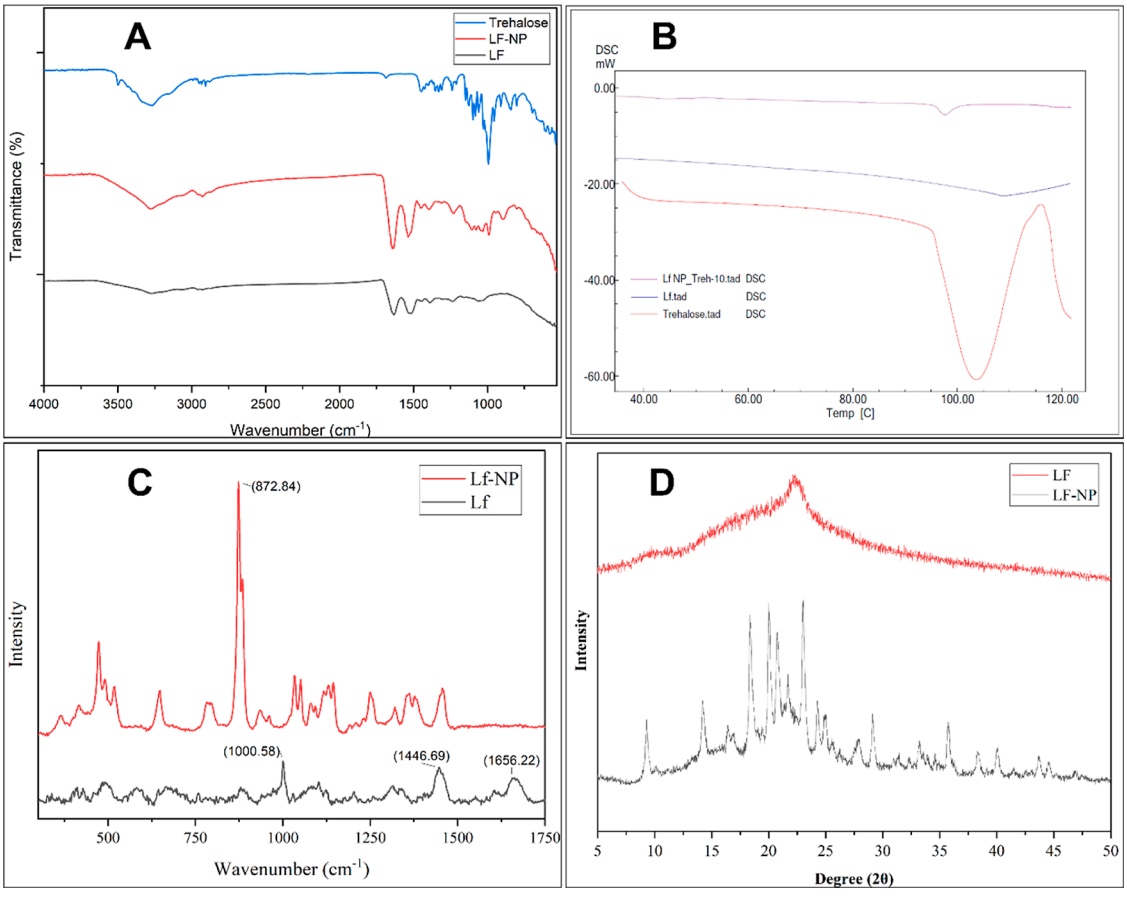

Figure 2. Spectral and thermal characterization of LF-NP: (A) FTIR spectra, (B) DSC plot, (C) Raman plot, and (D) XRD diffractogram.

https://doi.org/10.1021/acsomega.4c05991
ACS Omega 2024, 9, 42410−42422

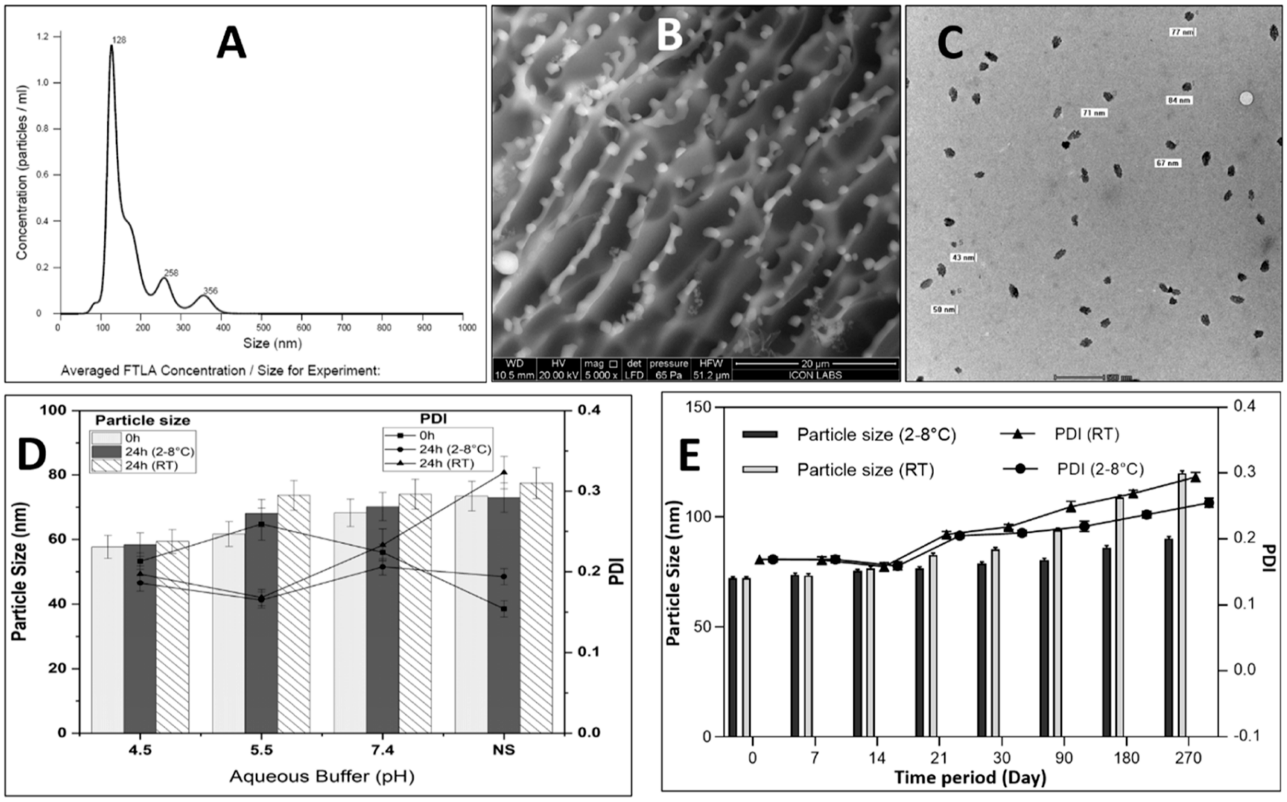

Figure 3. Characterization and stability evaluation of LF-NPs. (A) Concentration of LF-NPs from NTA plot, microscopic characterization of LF-NPs; (B) FESEM, (C) TEM, and stability of LF-NPs in (D) aqueous buffers of different pHs and (E) lyophilized samples stored at different temperatures.

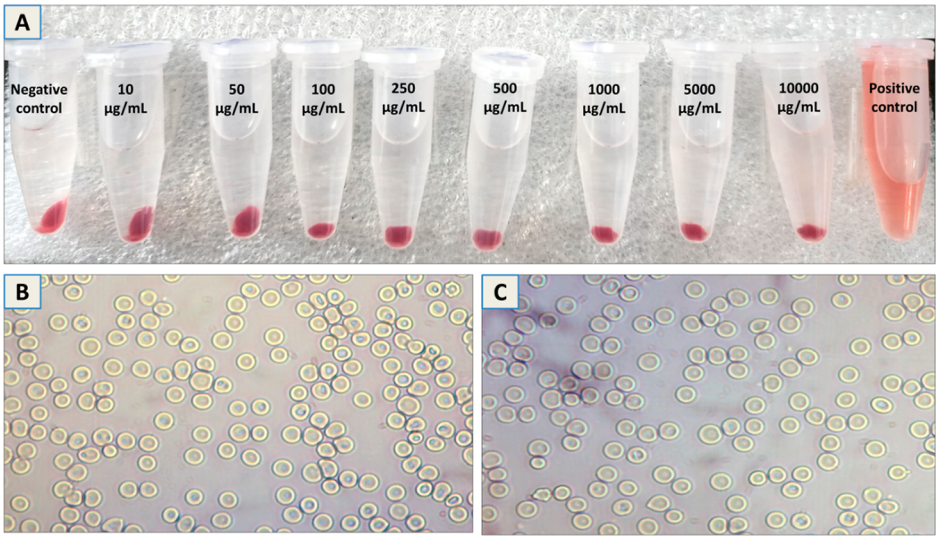

Figure 4. Hemocompatibility study of LF-NPs. (A) Hemolysis activity; microscopic images of RBCs treated with (B) PBS and (C) LF-NPs.

statistically significant. The exposed hydrophobic surfaces of LF-NPs during thermal treatment prevent their aggregation and stabilize the NPs.[21,22] Stability of nanoparticles is an important criterion vis-a-vis shelf life of the product. It was expected that LF-NPs, owing to the presence of sodium tripolyphosphate (cross-linking agent) in the composition, would be stable even at room temperature.[23] Details of the parameters analyzed are given in Figure 3E. It was observed that the sample stored under both refrigerated conditions and room temperature showed gradual increase in the particle size and PDI. Sadkin et al.'s review[24] of ^{99m}Tc-labeled nanocolloids states that the optimal size range for SLN targeting is 50−80 nm, which allows for efficient lymphatic drainage and accumulation in the SLN, enabling reliable mapping.[25] The obtained results indicate that under refrigerated conditions, the samples retained the size in the range of 60−80 nm even after 270 days, with a PDI < 0.25. This indicates the potential of LF-NPs to target the SLN even after 270 days of storage. However, the samples stored at room temperature crossed 100 nm after 180 days of storage with a PDI > 0.25. These results

https://doi.org/10.1021/acsomega.4c05991
ACS Omega 2024, 9, 42410−42422

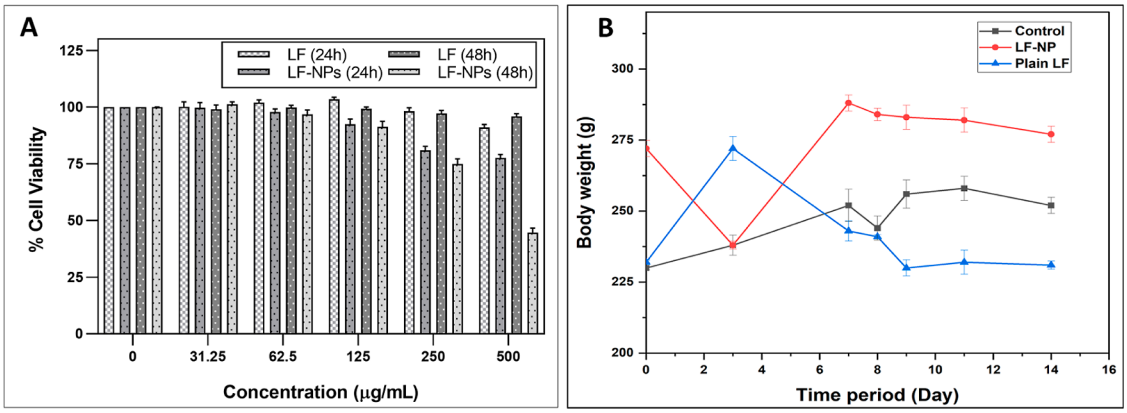

Figure 5. (A) Cytotoxicity evaluation of LF-NPs on RAW 264.7 cells. (B) Body weight changes of Wistar rats treated for acute toxicity study. All values are expressed as mean ± standard deviation, $n = 3$.

indicate that the product has significantly greater stability when stored under refrigeration.

2.5. Safety and Toxicity Profile of LF-NPs. *2.5.1. Hemocompatibility Evaluation.* Erythrocytes incubated with LF-NPs did not show noticeable hemolysis (<5%) at any of the tested concentrations ranging from 10 to 10^3 μg/mL (Figure 4A). Further, no changes were detected in the morphology of red blood cells (RBCs) at any of the tested concentrations (Figure 4C), comparable to the negative control profile (Figure 4B). These results indicate the absence of any detrimental interaction between RBCs and LF-NPs.

2.5.2. In Vitro Cytotoxicity Studies of LF-NPs on RAW-264.7 Cells. The in vitro cytotoxicity assay was performed on macrophages because of their role in the immune response and their ability to internalize NPs. It is vital for determining safety profile of the formulations, as they are frequently among the first cells to encounter nanoparticles in vivo.[26] The results shown in Figure 5A indicate that the cells treated with plain LF had almost no impact on the viability of the cells at all of the tested concentrations. The difference in cell viability suppression with time was not statistically significant at all the tested concentrations. Similarly, the cells treated with LF-NPs also showed minimum impact up to a concentration of 125 μg/mL, several orders greater than the concentration required for the intended application. Therefore, one can conclude that the formulation is not expected to induce any significant cytotoxicity after uptake in the SLN. These results are in agreement with earlier reports.[27]

2.5.3. In Vivo Toxicity Studies of the LF-NPs. The toxicity of LF-NPs was assessed in rats by administering the test molecules at a dose of 20 mg/kg via a subcutaneous route in the foot pad region. This route of administration mimics the procedure followed for the preclinical biological testing of SLN tracers. The safety profile of the NPs focused on key hematological parameters, biochemical markers, organ weights, and histopathology by comparing the LF-NPs treated animal groups with plain LF-treated animals.

The acute toxicity study showed that no considerable difference was observed with respect to the body weight (Figure 5B), dermal changes, and appearance of any ascites. Haematological parameters (Table 2) of all the treatment groups were comparable to that of the controls and the reference ranges.[28,29] After 14 days, serum was collected from test animals to assess the changes in biochemical parameters, and they were euthanized to study histopathological changes in major organs like liver, spleen, kidney, and heart. From Figure 6, it can be observed that all the serum biochemical parameters including kidney function markers and liver enzymes exhibited no deviations from the baseline levels,[30] indicating the absence of any acute toxicity. The histopathological studies (Figure 7), revealed the absence of any abnormalities in all the major organs studied. These results and observations collectively highlight the safety of LF-NPs and lay a strong basis for exploring their potential in SLN tracer applications.

2.6. Radiolabeling Studies of LF-NPs and Their Evaluation. Radioactive markers have distinct advantages over fluorescent markers, particularly in the context of photobleaching and tissue penetration. Fluorescent markers are often affected by photobleaching, where signal intensity diminishes over time with prolonged light exposure.[31] In comparison, radioisotopes are unaffected by the chemical environment and diagnostic radiotracers can be detected even when localized in deep-seated tissues.[32] ^{99m}Tc being a gamma emitter emits a low-energy γ radiation of 140.5 keV, which is optimal for gamma imaging and deposits minimal radiation dose in the subject.[33] Further, its half-life of 6 h allows for convenient use in imaging with no long-term radiation exposure. Radiolabeling of LF-NPs was optimized with respect to choice of buffer, incubation time, and concentration of reducing agent $SnCl_2$. Results of optimization studies are shown in Figure 8A−D. It was found that sodium acetate buffer (pH 5.4) gave a sharp peak at the point of spotting (POS) representing the radiolabeled LF-NPs. Meanwhile, phosphate buffer (pH 7.5) gave broader peaks spreading up to 4 cm from the POS (Figure 8A). These results were corroborated with the elution pattern from PD-10 size-exclusion chromatography: here, ^{99m}Tc-labeled LF-NPs are eluted out in the void volume, while the reduced ^{99m}Tc colloid is retained on the column until it is washed out with 5% hydrogen peroxide. PD-10 separation showed a comparable radiolabeling yield (Figure 8D). This indicated that sodium acetate buffer yielded better radiolabeling of the LF-NPs due to more stable ^{99m}Tc complex being formed around this pH. The effect of incubation time was assessed at 15, 30, and 60 min. It was observed that in all cases, more than 90% of the radioactivity was associated with the LF-NPs (Figure 8B). In the final stage of optimization, the effect of $SnCl_2$ concentration was evaluated. The results showed in Figure 8C indicate that for all the concentrations of $SnCl_2$ tried, the radiolabeling efficiency was approximately >94%, with the

https://doi.org/10.1021/acsomega.4c05991
ACS Omega 2024, 9, 42410−42422

Table 2. Haematological Parameters of Healthy Wistar Rats Treated with LF-NPs for Acute Toxicity Study[a]

		day 0			day 1			day 7		
parameters	normal range	control	plain LF	LF-NP	control	plain LF	LF-NP	control	plain LF	LF-NP
WBC × $10^3/\mu$L	4–21.6	13.93 ± 0.88	11.27 ± 0.13	11.17 ± 0.08	10.37 ± 0.71	10.4 ± 0.26	13.42 ± 1.6	13.57 ± 0.58	15.73 ± 0.54	12.17 ± 0.24
RBC × $10^6/\mu$L	6.4–9.1	6.92 ± 0.21	6.49 ± 0.12	8.61 ± 0.06	7.69 ± 0.41	7.45 ± 0.03	8.77 ± 0.36	7.51 ± 0.07	7.83 ± 0.2	7.67 ± 0.05
HGB × g/dL	8–17.2	10.3 ± 0.45	10.16 ± 0.15	12.77 ± 0.09	15.6 ± 0.33	15.03 ± 0.47	14.13 ± 1.08	11.79 ± 0.49	14.2 ± 0.73	13.6 ± 0.13
HCT × %	42.5–52.9	47.33 ± 0.65	36.53 ± 0.39	41.93 ± 0.48	49.83 ± 0.43	42.37 ± 1.18	46.8 ± 1.02	44.2 ± 0.98	45.3 ± 2.51	45.07 ± 1.59
MCV × fL	40–52.9	50.8 ± 0.42	52.53 ± 0.59	47.97 ± 0.1	47.63 ± 0.61	49.23 ± 0.14	48.37 ± 0.68	49.33 ± 0.52	50.13 ± 0.33	48.23 ± 0.08
MCH × pg	16.8–22.8	17.63 ± 0.31	15.93 ± 0.31	20.17 ± 0.28	19.07 ± 0.49	18.6 ± 0.19	17.63 ± 0.14	18.73 ± 0.16	17.33 ± 0.07	18.13 ± 0.26
MCHC × g/dL	29–34.6	31.2 ± 0.18	28.53 ± 0.47	31.17 ± 0.25	32.33 ± 1.08	31.77 ± 0.92	32.37 ± 0.83	32.93 ± 0.85	34.77 ± 0.1	32.2 ± 0.74
PLT × $10^3/\mu$L	668–1384	975.33 ± 49.22	1266 ± 4.02	1390.33 ± 3.51	747 ± 51.28	861.33 ± 15.74	716.67 ± 39.95	1105.33 ± 39.02	890 ± 13.54	745.33 ± 12.55
LY %	2.5–7.5	6.07 ± 0.21	7.6 ± 0.47	5.57 ± 0.04	4.87 ± 0.06	5.3 ± 0.11	5.9 ± 0.46	6.83 ± 0.24	6.3 ± 0.23	7.03 ± 0.04
MO %	0–0.8	0.33 ± 0.06	0.03 ± 0.01	0.1 ± 0.03	0.07 ± 0.03	0.2 ± 0.07	0.23 ± 0.05	0.27 ± 0.09	0.03 ± 0.01	0.27 ± 0.05
EO %	0–2.4	0.13 ± 0.01	0.93 ± 0.17	2.3 ± 0.09	0.47 ± 0.03	0.43 ± 0.09	1.3 ± 0.29	0.57 ± 0.05	2.27 ± 0.12	0.33 ± 0.1
GR %	0.6–4.3	2.6 ± 0.4	1.97 ± 0.05	2.43 ± 0.08	1.4 ± 0.16	3.67 ± 0.18	3.2 ± 0.36	3.33 ± 0.19	3.67 ± 0.1	3.2 ± 0.09
RDW-CV × %	0–50	15.23 ± 1.19	13.43 ± 0.09	12.87 ± 0.15	17.23 ± 1.33	14.3 ± 0.27	16.7 ± 0.98	14.9 ± 0.46	13.87 ± 0.09	13.67 ± 0.95
RDW-SD × fL	0–2.9	2.27 ± 0.11	22.97 ± 0.87	2.6 ± 0.03	1.54 ± 0.17	2.17 ± 0.1	2.07 ± 0.05	2.23 ± 0.1	2.36 ± 0.09	2.43 ± 0.1
PCT × %	0–20	1.29 ± 0.09	0.8 ± 0.09	1.09 ± 0.05	0.37 ± 0.05	0.59 ± 0.03	0.81 ± 0.1	1.15 ± 0.11	0.57 ± 0.05	0.84 ± 0.1
MPV × fL	0–50	6.77 ± 0.29	5.97 ± 0.05	7.63 ± 0.12	7.83 ± 0.56	7.1 ± 0.34	8 ± 0.7	6.5 ± 0.34	7.3 ± 0.31	8.36 ± 0.66
PDW × %	0–199	23.83 ± 1.9	20.17 ± 0.66	29.7 ± 1.24	44.6 ± 5.57	19.33 ± 0.63	15.97 ± 1.04	28.1 ± 1.26	18.7 ± 0.76	13.43 ± 0.6

[a]All values are given as mean ± standard deviation, $n = 3$.

https://doi.org/10.1021/acsomega.4c05991
ACS Omega 2024, 9, 42410−42422

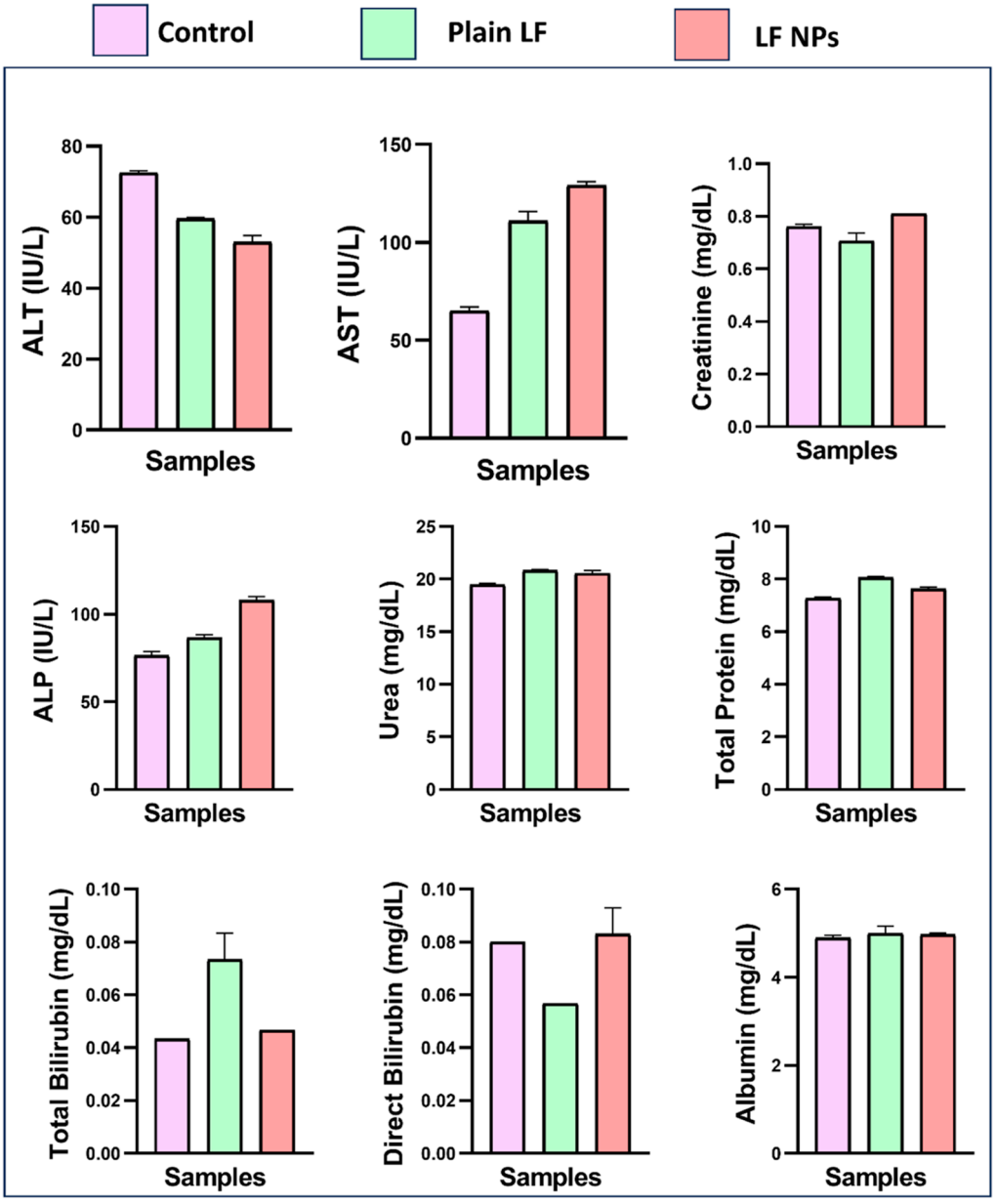

Figure 6. Serum biochemical parameters of Wistar rats treated for the acute toxicity study. All values are expressed as mean ± standard deviation, n = 3.

highest of 96.47% at 25 μg/mL. This may be attributed to the high density of primary amine groups present on the surface of LF-NPs, which efficiently form stable radiolabeled complex even at lower $SnCl_2$ concentrations. As tin(II) chloride has potential cytotoxicity, the lowest concentration (10 μg/mL) was chosen for further radiolabeling reactions.

The final optimized protocol involves dispersion of 1 mg of LF-NP in sodium acetate buffer (pH 5.4) followed by the addition of 10 μg of $SnCl_2$ and 37 MBq of $^{99m}TcO_4^-$. Final volume is adjusted to 1 mL using buffer and incubation is done for 30 min at room temperature. Using a combination of thin-layer chromatography (TLC) and size-based separation (PD-10), we determined >98% radiolabeling yield. The stability of ^{99m}Tc-LF-NP was assayed in both saline and serum. After the incubation, instant TLC (ITLC) was performed and the elution pattern was checked using a TLC radio scanner (Raytest, Germany). It was found that the ^{99m}Tc-labeled LF-NPs were stable in both saline and serum for >24 h.

2.7. In Vitro Uptake Studies of ^{99m}Tc-LF-NP. The in vitro uptake of ^{99m}Tc-LF-NPs in the RAW 264.7 cell line was studied with increasing concentrations of the formulation (Figure 8E). It was observed that ^{99m}Tc-LF-NPs exhibited concentration-dependent cellular uptake, with the highest uptake of 7.79 ± 1.73% observed at the concentration of 0.1 mg/mL. This trend in the cellular uptake of the LF-NPs indicates that with the increase in the concentration of the ^{99m}Tc-LF-NPs, the receptors available for uptake or the phagocytic capacity is saturated. Further studies on cellular internalization are required to study the detailed mechanism of uptake of LF-NPs by the cells.

LF interacts with CD14 and LPS binding protein for initial recognition and uptake by macrophages via the TLR4 pathway. This uptake, likely through endocytic pathways, is crucial for

https://doi.org/10.1021/acsomega.4c05991
ACS Omega 2024, 9, 42410−42422

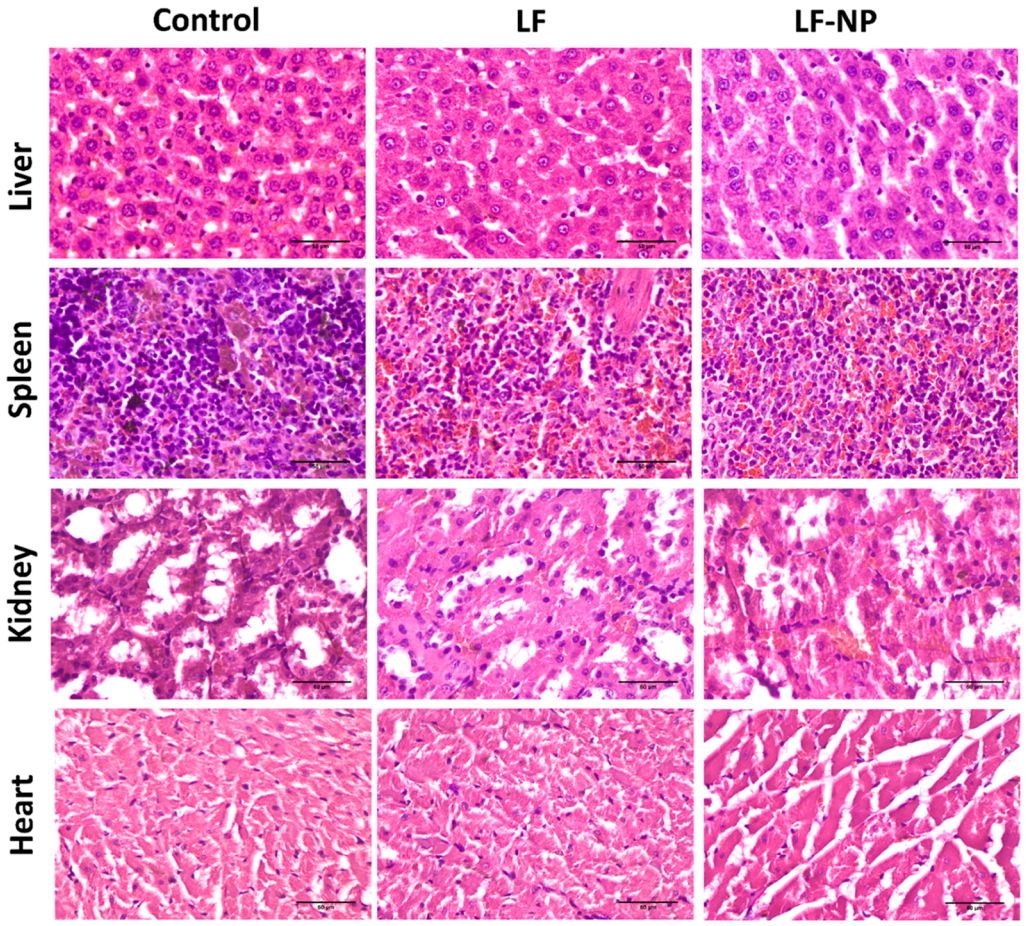

Figure 7. Histopathological images of major organs after treatment with LF-NPs.

triggering subsequent signaling events. The report of Curran et al.[34] details how LF activates macrophages via TLR4-dependent and independent pathways. Further, LF was reported to activate signaling components, such as NF-κB, p38, ERK, and JNK, independent of TLR4, indicating signaling through multiple intracellular pathways. The negative charge of LF-NPs influences their uptake through the lymphatic system. The irregular extracellular matrix of lymphatic vessels, which contains negatively charged glycosaminoglycans, may enhance the retention and entry of negatively charged nanoparticles like LF-NPs. Passive diffusion through the lymphatic endothelium, facilitated by the space between cells and lack of a basement membrane, allows for the entry of such NPs.[35] These factors provide additional leverage to LF-NPs to interact with macrophages, enabling their uptake.

2.8. In Vivo Biodistribution Studies of ^{99m}Tc-LF-NP. The in vivo biodistribution studies of ^{99m}Tc-LF-NP are depicted in Table 3. While the activity at the site of injection (footpad) is observed to decrease with time, we do not see a corresponding uptake in the popliteal (sentinel) node or the other nodes along the lymphatic channel. Given that the measured particle size of the LF-NPs is well within the optimal range for use in SLN detection, it suggests a possible agglomeration in vivo, which would greatly hamper the migration of LF-NPs from the site of injection. In vivo agglomeration of LF-NPs may occur due to interactions with tissue matrix, which can notably impact their in vivo kinetics and distribution. Studies[36,37] have shown that particle size can also influence the extent of agglomeration in the biological environment, wherein smaller nanoparticles may be more prone to agglomeration. In this study, an increase in radioactivity in the bloodstream over time was noticed. This suggests some form of degradation of the radioactive nanoparticles. If it were a case of TcO_4^- being released due to instability of the radiolabeling, then the bulk of the activity would be observed in the GI tract and cleared rapidly from the blood as per the expected distribution pattern for pertechnetate.[38] Soluble LF molecule again has a short plasma half-life (∼10 min): it is taken up in the liver and gall bladder and also excreted through the kidneys.[39] As the behavior observed herein does not reflect either of these phenomena, it would suggest that partial in vivo degradation is leading to the release of supramolecular fragments of the nanoparticles that are not retained within the lymph nodes but pass further into the bloodstream where they circulate for an extended period (at least 180 min p.i.). The precise nature of the degradation products is as yet unknown.

These limitations could be addressed by several approaches. For instance, PEGylation can potentially reduce the interaction with the tissue matrix at the site of injection, reducing agglomeration and enhancing the efficiency of SLN uptake. Studies[40] have reported that PEGylation enhances the hydrophilicity of the molecule, leading to enhanced uptake in the lymphatic system after subcutaneous injection. Another approach involves the addition of targeting ligands like mannose[41] that allow for selective binding to mannose receptors (CD206) highly expressed on macrophages and dendritic cells in SLNs. These strategies will serve as the

https://doi.org/10.1021/acsomega.4c05991
ACS Omega 2024, 9, 42410−42422

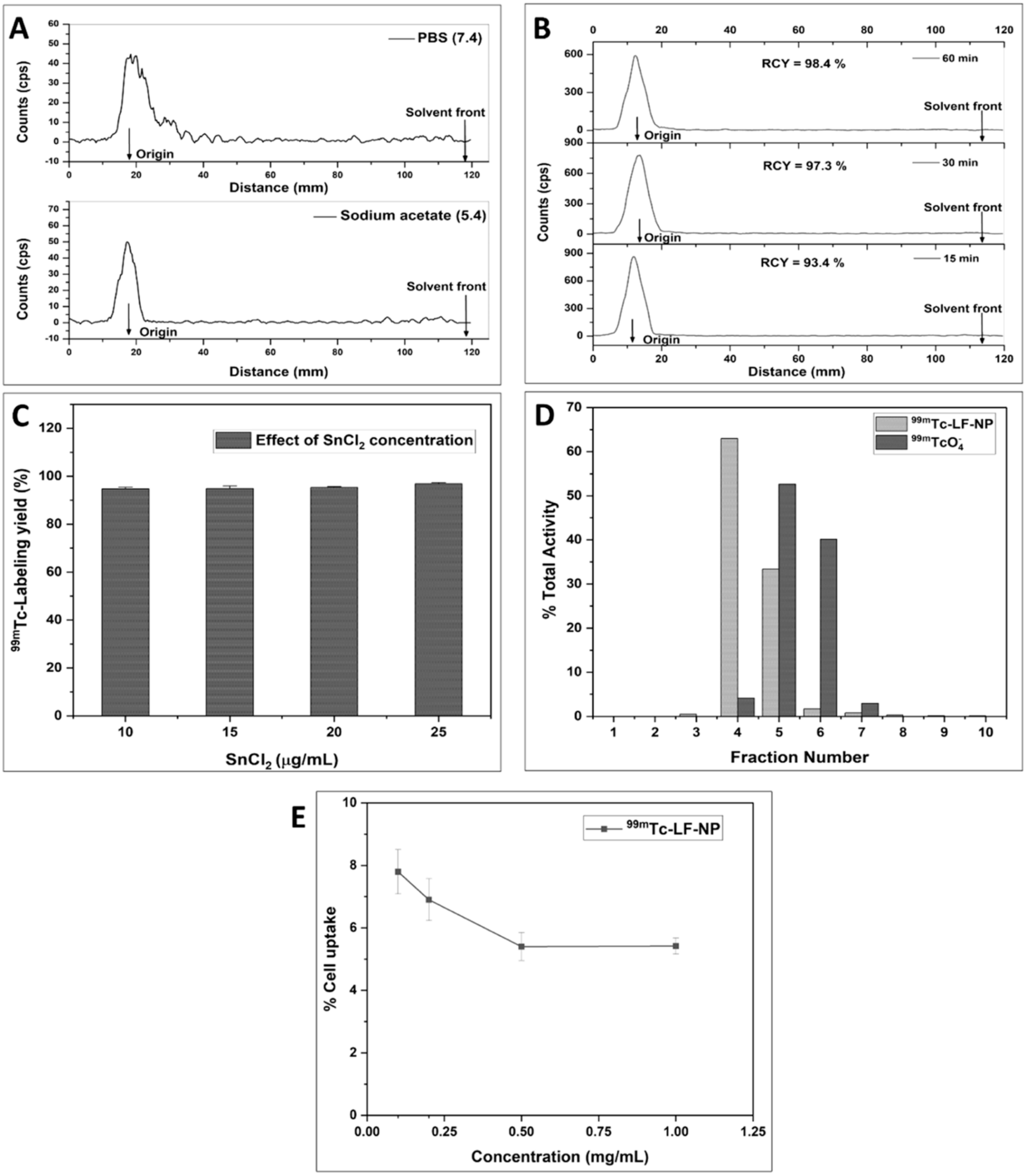

Figure 8. Radiolabeling of LF-NPs and its evaluation. (A) ITLC profiles comparing ^{99m}Tc-labeling of LF-NP in PBS and sodium acetate buffer, (B) effect of incubation time, (C) effect of $SnCl_2$ on the radiolabeling yield of ^{99m}Tc-LF-NP, (D) PD-10 elution profile, and (E) cellular uptake studies of ^{99m}Tc-LF-NP in RAW 264.7. All values are expressed as mean ± standard deviation, n = 3.

foundation for our future research, as we seek to improve the delivery efficiency of LF-NPs to SLNs.

3. MATERIALS AND METHODS

3.1. Materials. Bovine LF (Bioferrin 2000), was gifted by Glanbia Nutritionals, USA. ^{99m}Tc used for preparing radiolabeled nanoparticles was obtained as pertechnetate ($^{99m}TcO_4^-$) by elution with saline from an in-house ^{99}Mo-^{99m}Tc generator at the Radiopharmaceuticals Division, BARC. PD-10 columns (GE Healthcare) containing Sephadex G-25 resin were employed for labeled product separation. All other chemicals utilized were of reagent and analytical grade and were purchased from Sigma-Aldrich without further treatment.

3.2. Preparation of LF-NPs. LF-NPs were prepared via temperature-assisted coagulation method as previously reported by our team.[12] Briefly, LF was dissolved in Milli-Q grade water, and the pH of this solution was adjusted to pH 7.0 using a 0.1 N NaOH or 0.1 N HCl solution. The effect of different monovalent (NaCl and KCl), divalent (d-SHP), and

https://doi.org/10.1021/acsomega.4c05991
ACS Omega 2024, 9, 42410−42422

Table 3. In Vivo Biodistribution of ^{99m}Tc-LF-NP in Wistar Rat Model[a]

time	15 min	30 min	60 min	180 min
		Organ		
liver	0.15 ± 0.05	0 ± 0	0.03 ± 0.22	0.02 ± 0.01
intestine	0.08 ± 0.03	0.01 ± 0	0.19 ± 0.26	0.21 ± 0.1
kidney	0.24 ± 0.07	0 ± 0	0.45 ± 0.32	2.42 ± 0.66
heart	0.08 ± 0.01	0 ± 0	0.03 ± 0.18	0 ± 0
lungs	0.12 ± 0.04	0 ± 0	0.05 ± 0.29	0.24 ± 0.12
spleen	0.06 ± 0.05	0 ± 0	0.11 ± 0.13	0.22 ± 0.11
blood	13.88 ± 0.37	19.97 ± 1.28	19.41 ± 1.99	35.75 ± 8.25
stomach	0.07 ± 0.1	0 ± 0	0.06 ± 0.03	0.15 ± 0
		Node Uptake		
popliteal node	0.34 ± 0.28	0.02 ± 0	0.13 ± 0.18	0.34 ± 0.11
iliac node	0.17 ± 0.1	0.08 ± 0	0.05 ± 0.11	0 ± 0
site of injection	84.25 ± 0.07	79.79 ± 2.81	78.82 ± 1.26	60.42 ± 0.99

[a]All values are given % ID/organ and expressed as mean ± standard deviation, n = 3.

polyvalent salts [SC and sodium tripolyphosphate (TPP)] at a concentration of ∼2 mM was assessed on the formation LF-NPs. Later, the solution was subjected to optimized conditions of reaction at 75 °C for 15−20 min to form the nanoparticles. The obtained nanoparticles were freeze-dried and used for characterization studies.

3.3. Freeze-Drying of LF-NPs and Reconstitution of the Freeze-Dried Products. The obtained NPs were freeze-dried in the Christ Alpha 1−2 LDplus lyophilizer (Martin-Christ, Germany). The samples were subjected to freeze-drying for 48 h at −55 °C and pressure <0.1 mbar. To optimize use of cryoprotectants, various cryoprotectants across a concentration gradient were tested with the NP suspension. The final freeze-dried products were reconstituted with double-distilled water and the rehydration was visually observed after gentle agitation. The reconstitution time and appearance of the reconstituted product were noted prior to studying critical parameters like particle size and zeta potential of the suspension.

3.4. Characterization of Nanoparticles. The particle size, PDI, and zeta potential of the nanoparticles were assessed using a Malvern Zetasizer (Zetasizer Nano ZS, Malvern Instruments Inc., Malvern, UK). Nanoparticle concentration was determined using a Nanoparticle Tracking Analyzer (Nanosight Malvern LM14). Captured images were analyzed by software (NTA 3.4 Build 3.4.003) to determine the particle size and concentration. To examine changes in the chemical nature of the protein structure, FTIR spectra of LF powder and thermally treated LF-NPs were obtained using the Attenuated Total Reflectance technique (Instrument: Bruker Alpha II, US), by scanning in the range of 400−4000 cm^{-1}. DSC analysis (DSC-60 Plus, Shimadzu, Japan) was performed by sealing the samples in the aluminum pan and heating them under nitrogen flow (40 mL/min) with a heating rate of 10 °C/min from 30 to 120 °C. Spectroscopic techniques like XRD were performed to understand the changes in their crystallinity. Morphological attributes of the synthesized nanoparticles were studied by using SEM and TEM.

3.5. Stability of LF-NPs. The LF-NPs were dispersed and incubated in different pH media to understand their stability. Briefly, 1 mg of LF-NP was dispersed in 1 mL of different aqueous buffers (pH 4.5, 5.5, 7.4, and NS) and incubated for 24 h. The changes in particle size and zeta potential were studied using a Malvern Zetasizer. Further, the storage stability of the freeze-dried formulation was studied in a stability chamber (Thermolab instruments, TH 500 G) by subjecting the samples to refrigerated conditions (2−8 °C) and room temperature (25 ± 2 °C, 60% ± 5% RH). At specific time points, the sample was redispersed in Milli-Q water to check the variations in particle size and zeta potential.

3.6. Safety and Toxicity Profile of LF-NPs. *3.6.1. Hemocompatibility Evaluation.* The hemocompatibility studies was performed similar to our earlier reports.[12,42,43] Briefly, blood collected from Wistar rats was centrifuged at 4000 rpm for 5 min to harvest the RBCs. They were washed twice with phosphate-buffered saline (PBS) at 2500 rpm for 5 min. The collected RBC concentrate was diluted 10 times with PBS at 7.4. Then, the Lf-NP formulation was added, sample concentration ranging from 0.01 to 2.0 mg/mL. RBCs treated with PBS and 2% v/v Triton X-100 served as negative and positive controls, respectively. The treated samples were incubated in a shaking incubator at 37.5 ± 2 °C for 2 h and then centrifuged at 2500 rpm for 5 min to separate the RBC.[44,45] The absorbance (A) of the supernatant was measured at 541 nm, and % hemolysis was calculated using the below equation. Morphological changes in the treated RBCs were checked (Motic, BA400, China).

$$\%\ \text{haemolysis} = \frac{|A(\text{sample})| - |A(\text{negative control})|}{|A(\text{positive control})| - |A(\text{negative control})|} \times 100$$

3.6.2. In Vitro Cytotoxicity Studies of LF-NPs on RAW-264.7 Cells. In targeting the SLN, nanoparticles get engulfed by the macrophages present in SLN and are expected to be retained in the node for at least some hours. Therefore, it is useful to evaluate the potential cytotoxicity to macrophages from nanoparticles designed to target SLN. In this study, RAW 264.7 macrophage precursor cells were selected to evaluate the cytotoxicity of LF-NPs. RAW 264.7 cells obtained from the repository of the National Centre for Cell Science, India, were cultured in Dulbecco's modified Eagle's medium (DMEM) containing 10% fetal bovine serum (FBS) as a growth supplement. After harvesting adequate cell numbers, they were seeded into 96-well plates and treated with varying concentrations of plain LF and LF-NPs for 24 and 48 h. After the specified treatment periods, the MTT assay was performed, resulting in the formation of formazan crystals. These were solubilized by using dimethyl sulfoxide, and their absorbance was measured at 570 nm using a spectrophotometer. The

https://doi.org/10.1021/acsomega.4c05991
ACS Omega 2024, 9, 42410−42422

resulting data were analyzed to determine the IC50 values for LF and LF-NPs at both time points.

3.6.3. In Vivo Toxicity Studies of the LF-NPs. All animal studies were performed following the regulations established by CPCSEA and were approved by the Institutional Animal Ethics Committee, KMC, Manipal (94/PO/RReBi/S/99/CPCSEA), India. Acute toxicity studies of LF-NPs were performed in healthy female Wistar rats (6−8 weeks old, 200−300 g). No specific influence of gender is expected on the results from the experimental design. The rats were housed in cages for acclimatization before the initiation of studies. For toxicity studies, the rats were randomly divided into four groups (n = 3), i.e., group-1: control, group-2: plain LF, and group-3: LF-NPs. Rats were subcutaneously administered in the foot pad region with 20 mg/kg of the material, at least 10-fold higher than the dose proposed to be used for the intended application. Different biochemical parameters indicating the effect of treatment on major organs like liver (alanine aminotransferase, albumin, alkaline phosphatase, aspartate aminotransferase, total bilirubin, and total protein) and kidney (creatinine and urea) were analyzed after 14 days of treatment. Other parameters like hematological parameters, changes in body weight, impaired mobility, presence of ascites, or visible dermal changes were also monitored. Subsequently, the animals were euthanized to collect tissue samples from major organs like liver, spleen, kidney, and heart; the tissues were immersed in a 10% formalin solution for 48 h to facilitate histopathological studies. Formalin fixed tissue lobes were embedded in paraffin and stained with hematoxylin and eosin. Microscopic examination of the test and control specimens was carried out using a trinocular research microscope (LX-500 light-emitting diode, Labomed), and images were captured using a microscope camera (MiaCam CMOS AR 6pro).

3.7. Radiolabeling Studies of LF-NP and Its Evaluation. The direct radiolabeling of the NPs with ^{99m}Tc involves the reduction of TcO_4^- in the presence of the LF-NPs using stannous chloride as a reducing agent. Preliminary investigation of ^{99m}Tc-labeling of LF-NP was done using "one factor at a time" approach. Factors like choice of buffer, incubation time, concentration of $SnCl_2$, and temperature were assessed.[46] To perform radiolabeling, 1 mg of lyophilized LF-NP was reconstituted in 1 mL of reaction buffer, and ∼10 MBq of ^{99m}Tc was added. $SnCl_2$ in an aqueous solution (10 μg/mL) was added to the dispersion and vortexed to mix thoroughly. The labeling reaction was carried out at room temperature for 30 min. The ^{99m}Tc-labeled product was then purified by using a PD-10 column. Bradford protein assay of eluted fractions was performed to identify the fractions containing LF-NP. Radiochemical yield of the reaction mixture was assessed using ITLC. We used 0.9% (w/v) saline as mobile phase for ITLC, where the labeled NP and ^{99m}Tc colloids remain at the POS (R_f = 0) and free $^{99m}TcO^{4-}$ moves toward solvent front (R_f = 0.8−0.9), and the TLC strips were scanned using a radio-TLC scanner (miniGita, Raytest, Germany). This was correlated with the elution fractions from PD-10 size-exclusion column, which were measured on a NaI (Tl) scintillation counter (Mucha, Raytest, Germany); here, ^{99m}Tc-labeled LF-NP was eluted in the void volume, free $^{99m}TcO^{4-}$ emerged later and reduced/colloidal ^{99m}Tc was retained in the column until washed out using dilute aqueous hydrogen peroxide solution. To determine stability of the ^{99m}Tc-LF-NP, the complex was diluted at 1:10 with saline (% vol/vol) at a final volume of 500 μL and incubated at 37 °C. After the incubation, ITLC was performed as described above at different time points of 1, 3, and 24 h. Similarly, stability of the complex in blood serum was also assessed.

3.8. In Vitro Uptake Studies of ^{99m}Tc-LF-NP. The in vitro uptake study of ^{99m}Tc-LF-NP was performed by using RAW 264.7 cells. The cells were cultured at 37 °C with 5% CO_2 atmosphere in DMEM growth medium supplemented with 10% FBS. For the experiment, the cells were seeded in 24-well plates at a density of 10^6 cells/well and incubated for 24 h to allow for adhesion and monolayer formation. To assess the uptake of ^{99m}Tc-labeled LF-NP by macrophage cells, a saturation binding assay was performed. Increasing concentrations of the radiotracer (0.1 to 1.0 mg/mL LF-NP) were added to RAW 264.7 cells and incubated for 2 h at 37 °C. The assay was conducted in triplicate. After incubation, the supernatant was aspirated carefully, and the cells were washed twice with ice-cold PBS. The cell monolayer was then dissolved by the addition of 0.1 M NaOH. Cell lysates were collected into counting tubes and the associated radioactivity was measured using a NaI (Tl) scintillation counter.

3.9. In Vivo Biodistribution Studies of ^{99m}Tc-LF-NP. All animal studies adhered to the regulations established by the national regulatory body CPCSEA and were approved by the Institutional Animal Ethics Committee. The preclinical biological evaluation of ^{99m}Tc labeled LF-NPs was done by carrying out biodistribution studies in healthy female Wistar rats. No specific influence of gender is expected on the results from the experimental design. Following our previously reported protocol, the footpad model was used to evaluate the ability of LF-NPs to be taken up and retained in the SLN.[47] Under anesthesia using Ketamine/Xylazine (10:1), 50 μL of ^{99m}Tc-LF-NP suspension was administered subcutaneously into the footpad of the animal to track its uptake into the popliteal (sentinel) node and further up the lymphatic channel. They were housed under normal conditions for designated time-points (15, 30, 60, and 180 min). At 5 min prior to the end of each time point, methylene blue dye was administered into the footpad in an identical manner to provide visual indication of the lymph nodes. At the respective end-points, animals were sacrificed by CO_2 saturation, and relevant organs/tissues were excised. Radioactivity associated with each organ was measured on a flatbed type NaI (Tl) scintillation detector (Harshaw, USA). The accumulated radioactivity in the different organs was converted to a percentage of the total administered activity dose per organ (% ID/organ). Blood was extrapolated to account for 7% of the body weight.

4. SUMMARY AND CONCLUSIONS

In the current report, a simple and efficient method was optimized for preparation of LF-NPs using TPP cross-linker, toward potential use as a particulate radiotracer for SLN detection. The synthesized nanoformulation showed a favorable particle size range of 60−80 nm in particle size (PDI < 0.2) and was found to be stable for over 60 days at RT. In vitro and in vivo toxicity assays confirmed its biocompatibility. Radiolabeling studies showed that the LF-NPs could be labeled with the diagnostic radiolabel ^{99m}Tc with an efficiency >95%, and showed sufficient in vitro stability. The ^{99m}Tc-LF-NPs showed appreciable (>6%) uptake in RAW 264.7 macrophage precursor cells indicating a potential ability to be retained in SLNs. However, biodistribution studies performed in Wistar rats did not show corresponding SLN

https://doi.org/10.1021/acsomega.4c05991
ACS Omega 2024, 9, 42410−42422

uptake of the formulation, and the results indicated possible fragmentation of the nanoparticles in vivo. This suggests the need for a modification of the nanomaterial to render it more stable for in vivo SLN detection. PEGylation of the LF nanocarrier to render it more resistant to biological degradation is one possible approach, and this will be taken up for further work toward developing suitable a SLN radiotracer with this material.

AUTHOR INFORMATION

Corresponding Authors

Suresh Subramanian − *Radiopharmaceuticals Division, Bhabha Atomic Research Centre, Mumbai, Maharashtra State 400085, India*; Email: sursub@barc.gov.in

Srinivas Mutalik − *Department of Pharmaceutics, Manipal College of Pharmaceutical Sciences, Manipal Academy of Higher Education, Manipal 576104 Karnataka, India*; orcid.org/0000-0002-0642-1928; Email: ss.mutalik@manipal.edu

Authors

Sanjay Kulkarni − *Department of Pharmaceutics, Manipal College of Pharmaceutical Sciences, Manipal Academy of Higher Education, Manipal 576104 Karnataka, India*

Anuj Kumar − *Radiopharmaceuticals Division, Bhabha Atomic Research Centre, Mumbai, Maharashtra State 400085, India*

Abhijeet Pandey − *Department of Pharmaceutics, Manipal College of Pharmaceutical Sciences, Manipal Academy of Higher Education, Manipal 576104 Karnataka, India; Global Drug Development/Technical Research and Development, Novartis Healthcare Pvt. Ltd., Hyderabad 500081, India*

Soji Soman − *Department of Pharmaceutics, Manipal College of Pharmaceutical Sciences, Manipal Academy of Higher Education, Manipal 576104 Karnataka, India*

Complete contact information is available at: https://pubs.acs.org/10.1021/acsomega.4c05991

Author Contributions

Sanjay Kulkarni: methodology, formal analysis, data curation, and writing—original draft. Anuj Kumar: methodology, formal analysis, data curation, and writing—original draft. Abhijeet Pandey: conceptualization, formal analysis, data curation, and writing—review and editing. Soji Soman: methodology, formal analysis, data curation, and writing—original draft. Suresh Subramanian: conceptualization, validation, data curation, writing—review and editing, project administration, and resources. Srinivas Mutalik: conceptualization, validation, data curation, supervision, writing—review and editing, project administration, and resources. All of the authors have read and approved the final manuscript.

Notes

The authors declare no competing financial interest.

The views and opinions expressed in this article are purely those of the authors and do not necessarily reflect the official policy or position of author's employer (Novartis Healthcare) or any of Novartis officers.

ACKNOWLEDGMENTS

The authors are thankful to—(i) Board of Research in Nuclear Science (BRNS), Department of Atomic Energy, Government of India, New Delhi for providing the research grant (no. 54/14/06/2021-BRNS/10342) to S.M. and Senior Research Fellowship to S.K., (ii) Department of Science and Technology (DST), Government of India, New Delhi, for providing INSPIRE Senior Research Fellowship to S.S. (INSPIRE Fellowship Code No. IF190328), (iii) Manipal Academy of Higher Education, Manipal (for providing Postdoctoral Research Fellowship to A.P.), (iv) Radiochemicals Section, Radiopharmaceuticals Division and Shri Krishnamohan Repaka, Board of Radiation and Isotope Technology for arranging to provide Tc-99m used in the work, and (v) Manipal College of Pharmaceutical Sciences, Manipal Academy of Higher Education, Manipal and Bhabha Atomic Research Centre, Mumbai for providing the facilities and support.

REFERENCES

(1) Lee, J.; Kang, S.; Park, H.; Sun, J. G.; Kim, E. C.; Shim, G. Nanoparticles for Lymph Node-Directed Delivery. *Pharmaceutics* **2023**, *15* (2), 565.

(2) McCright, J.; Naiknavare, R.; Yarmovsky, J.; Maisel, K. Targeting Lymphatics for Nanoparticle Drug Delivery. *Front. Pharmacol* **2022**, *13*, 887402.

(3) Liu, B.; Newburg, D. S. Human Milk Glycoproteins Protect Infants against Human Pathogens. *Breastfeed. Med.* **2013**, *8* (4), 354−362.

(4) Cutone, A.; Rosa, L.; Ianiro, G.; Lepanto, M. S.; Bonaccorsi di Patti, M. C.; Valenti, P.; Musci, G. Lactoferrin's Anti-Cancer Properties: Safety, Selectivity, and Wide Range of Action. *Biomolecules* **2020**, *10* (3), 456.

(5) Mattia, D. A. Use of Bovine Milk-derived Lactoferrin In Term Milk-based Infant Formulas and Toddler; GRAS Notice (GRN) No. 669, Cow's milk-derived lactoferrin. https://www.fda.gov/media/124472/download (accessed Feb 03, 2024).

(6) Administration (TGA). T. G. Lactoferrin (353391)|Therapeutic Goods Administration (TGA). https://www.tga.gov.au/resources/artg/353391 (accessed Feb 03, 2024).

(7) Safety of "Bovine Lactoferrin"|EFSA. https://www.efsa.europa.eu/en/efsajournal/pub/2701 (accessed Feb 03, 2024).

(8) Telang, S. Lactoferrin: A Critical Player in Neonatal Host Defense. *Nutrients* **2018**, *10* (9), 1228.

(9) Curran, C. S.; Demick, K. P.; Mansfield, J. M. Lactoferrin Activates Macrophages via TLR4-Dependent and -Independent Signaling Pathways. *Cell. Immunol.* **2006**, *242* (1), 23−30.

(10) Banerjee, S.; Pillai, M. R. A.; Ramamoorthy, N. Evolution of Tc-99m in Diagnostic Radiopharmaceuticals. In *Seminars in Nuclear Medicine*; Elsevier, 2001; Vol. *31*, pp 260−277.

(11) AAC07056269. *Technetium-99m Radiopharmaceuticals: Manufacture of Kits*; Internat. Atomic Energy Agency, 2008.

(12) Kulkarni, S.; Pandey, A.; Nikam, A. N.; Nannuri, S. H.; George, S. D.; Fayaz, S. M. A.; Vincent, A. P.; Mutalik, S. ZIF-8 Nano Confined Protein-Titanocene Complex Core-Shell MOFs for Efficient Therapy of Neuroblastoma: Optimization, Molecular Dynamics and Toxicity Studies. *Int. J. Biol. Macromol.* **2021**, *178*, 444−463.

(13) Martins, J. T.; Santos, S. F.; Bourbon, A. I.; Pinheiro, A. C.; González-Fernández, Á.; Pastrana, L. M.; Cerqueira, M. A.; Vicente, A. A. Lactoferrin-Based Nanoparticles as a Vehicle for Iron in Food Applications-Development and Release Profile. *Food Res. Int.* **2016**, *90*, 16−24.

(14) Sabra, S.; Agwa, M. M. Lactoferrin, a Unique Molecule with Diverse Therapeutical and Nanotechnological Applications. *Int. J. Biol. Macromol.* **2020**, *164*, 1046−1060.

(15) Singh, J.; Sharma, M.; Jain, N.; Aftab, I.; Vikram, N.; Singh, T. P.; Sharma, P.; Sharma, S. Lactoferrin and Its Nano-Formulations in Rare Eye Diseases. *Indian J. Ophthalmol.* **2022**, *70* (7), 2328−2334.

(16) Jonassen, H.; Treves, A.; Kjøniksen, A.-L.; Smistad, G.; Hiorth, M. Preparation of Ionically Cross-Linked Pectin Nanoparticles in the

Presence of Chlorides of Divalent and Monovalent Cations. *Biomacromolecules* **2013**, *14* (10), 3523−3531.
(17) Jiménez-Barrios, P.; Jaén-Cano, C. M.; Malumbres, R.; Cilveti-Vidaurreta, F.; Bellanco-Sevilla, A.; Miralles, B.; Recio, I.; Martínez-Sanz, M. Thermal Stability of Bovine Lactoferrin Prepared by Cation Exchange Chromatography and Its Blends with Authorized Additives for Infant Formulas. *Lebensm. Wiss. Technol.* **2022**, *154*, 112744.
(18) Duarte, L. G. R.; Ferreira, N. C. A.; Fiocco, A. C. T. R.; Picone, C. S. F. Lactoferrin-Chitosan-TPP Nanoparticles: Antibacterial Action and Extension of Strawberry Shelf-Life. *Food Bioprocess Technol.* **2023**, *16* (1), 135−148.
(19) Zavatski, S.; Khinevich, N.; Girel, K.; Redko, S.; Kovalchuk, N.; Komissarov, I.; Lukashevich, V.; Semak, I.; Mamatkulov, K.; Vorobyeva, M.; et al. Surface Enhanced Raman Spectroscopy of Lactoferrin Adsorbed on Silvered Porous Silicon Covered with Graphene. *Biosensors* **2019**, *9* (1), 34.
(20) Abazari, A.; Chakraborty, N.; Hand, S.; Aksan, A.; Toner, M. A Raman Microspectroscopy Study of Water and Trehalose in Spin-Dried Cells. *Biophys. J.* **2014**, *107* (10), 2253−2262.
(21) Bengoechea, C.; Peinado, I.; McClements, D. J. Formation of Protein Nanoparticles by Controlled Heat Treatment of Lactoferrin: Factors Affecting Particle Characteristics. *Food Hydrocolloids* **2011**, *25* (5), 1354−1360.
(22) March, D.; Bianco, V.; Franzese, G. Protein Unfolding and Aggregation near a Hydrophobic Interface. *Polymers* **2021**, *13* (1), 156.
(23) Yang, S.; Dai, L.; Mao, L.; Liu, J.; Yuan, F.; Li, Z.; Gao, Y. Effect of Sodium Tripolyphosphate Incorporation on Physical, Structural, Morphological and Stability Characteristics of Zein and Gliadin Nanoparticles. *Int. J. Biol. Macromol.* **2019**, *136*, 653−660.
(24) Sadkin, V.; Sкuridin, V.; Nesterov, E.; Stasyuk, E.; Rogov, A.; Varlamova, N.; Zelchan, R. 99mTc-Labeled Nanocolloid Drugs: Development Methods. *Sci. Rep.* **2020**, *10* (1), 14013.
(25) Agency, I. A. E. Radiopharmaceuticals for Sentinel Lymph Node Detection: Status and Trends; Text; International Atomic Energy Agency, 2015; pp 1−162. https://www.iaea.org/publications/10713/radiopharmaceuticals-for-sentinel-lymph-node-detection-status-and-trends (accessed Sept 10, 2023).
(26) Niu, Y.; Tang, M. In vitro Review of Nanoparticles Attacking Macrophages: Interaction and Cell Death. *Life Sci.* **2022**, *307*, 120840.
(27) Anand, N.; Kanwar, R. K.; Dubey, M. L.; Vahishta, R. K.; Sehgal, R.; Verma, A. K.; Kanwar, J. R. Effect of Lactoferrin Protein on Red Blood Cells and Macrophages: Mechanism of Parasite–-Host Interaction. *Drug Des., Dev. Ther.* **2015**, *9*, 3821−3835.
(28) Wang, W.; Dong, Z.; Zhang, J.; Zhou, X.; Wei, X.; Cheng, F.; Li, B.; Zhang, J. Acute and Subacute Toxicity Assessment of Oxyclozanide in Wistar Rats. *Front. Vet. Sci.* **2019**, *6*, 294.
(29) Delwatta, S. L.; Gunatilake, M.; Baumans, V.; Seneviratne, M. D.; Dissanayaka, M. L. B.; Batagoda, S. S.; Udagedara, A. H.; Walpola, P. B. Reference Values for Selected Hematological, Biochemical and Physiological Parameters of Sprague-Dawley Rats at the Animal House, Faculty of Medicine, University of Colombo, Sri Lanka. *Anim. Models Exp. Med.* **2018**, *1* (4), 250−254.
(30) Interspecies Database. https://www.interspeciesinfo.com/ (accessed Oct 07, 2023).
(31) Thorley, J. A.; Pike, J.; Rappoport, J. Z. Super-Resolution Microscopy: A Comparison of Commercially Available Options. In *Fluorescence Microscopy*; Cornea, A., Conn, P. M., Eds.; Academic Press: Boston, 2014; Chapter 14, pp 199−212.
(32) Lázaro-Ibáñez, E.; Faruqu, F. N.; Saleh, A. F.; Silva, A. M.; Tzu-Wen Wang, J.; Rak, J.; Al-Jamal, K. T.; Dekker, N. Selection of Fluorescent, Bioluminescent, and Radioactive Tracers to Accurately Reflect Extracellular Vesicle Biodistribution in vivo. *ACS Nano* **2021**, *15* (2), 3212−3227.
(33) Kane, S. M.; Padda, I. S.; Patel, P.; Davis, D. D. Technetium-99m. In *StatPearls*; StatPearls Publishing: Treasure Island (FL), 2024.
(34) Curran, C. S.; Demick, K. P.; Mansfield, J. M. Lactoferrin Activates Macrophages via TLR4-Dependent and -Independent Signaling Pathways. *Cell. Immunol.* **2006**, *242* (1), 23−30.
(35) Tang, Y.; Liu, B.; Zhang, Y.; Liu, Y.; Huang, Y.; Fan, W. Interactions between Nanoparticles and Lymphatic Systems: Mechanisms and Applications in Drug Delivery. *Adv. Drug Delivery Rev.* **2024**, *209*, 115304.
(36) Ha, M. K.; Shim, Y. J.; Yoon, T. H. Effects of Agglomeration on in vitro Dosimetry and Cellular Association of Silver Nanoparticles. *Environ. Sci.: Nano* **2018**, *5* (2), 446−455.
(37) Murugadoss, S.; Brassinne, F.; Sebaihi, N.; Petry, J.; Cokic, S. M.; Van Landuyt, K. L.; Godderis, L.; Mast, J.; Lison, D.; Hoet, P. H.; van den Brule, S. Agglomeration of Titanium Dioxide Nanoparticles Increases Toxicological Responses in vitro and in vivo. *Part. Fibre Toxicol.* **2020**, *17*, 10.
(38) Valenca, S. S.; Lima, E. A.; Dire, G. F.; Bernardo-Filho, M.; Porto, L. C. Sodium Pertechnetate (Na99mTcO4) Biodistribution in Mice Exposed to Cigarette Smoke. *BMC Nucl. Med.* **2005**, *5*, 1.
(39) Elzoghby, A. O.; Abdelmoneem, M. A.; Hassanin, I. A.; Abd Elwakil, M. M.; Elnaggar, M. A.; Mokhtar, S.; Fang, J.-Y.; Elkhodairy, K. A. Lactoferrin, a Multi-Functional Glycoprotein: Active Therapeutic, Drug Nanocarrier & Targeting Ligand. *Biomaterials* **2020**, *263*, 120355.
(40) McCright, J.; Skeen, C.; Yarmovsky, J.; Maisel, K. Nanoparticles with Dense Poly(Ethylene Glycol) Coatings with near Neutral Charge Are Maximally Transported across Lymphatics and to the Lymph Nodes. *Acta Biomater.* **2022**, *145*, 146−158.
(41) Jirátová, M.; Gálisová, A.; Rabyk, M.; Sticová, E.; Hrubý, M.; Jirák, D. Mannan-Based Nanodiagnostic Agents for Targeting Sentinel Lymph Nodes and Tumors. *Molecules* **2021**, *26* (1), 146.
(42) Nannuri, S. H.; Pandey, A.; Kulkarni, S.; Deshmukh, P. K.; George, S. D.; Mutalik, S. A New Paradigm in Biosensing: MOF-Carbon Dot Conjugates. *Mater. Today Commun.* **2023**, *35*, 106340.
(43) Pandey, A.; Kulkarni, S.; Vincent, A. P.; Nannuri, S. H.; George, S. D.; Mutalik, S. Hyaluronic Acid-Drug Conjugate Modified Core-Shell MOFs as pH Responsive Nanoplatform for Multimodal Therapy of Glioblastoma. *Int. J. Pharm.* **2020**, *588*, 119735.
(44) Wang, H.; Yang, Z.; He, Z.; Zhou, C.; Wang, C.; Chen, Y.; Liu, X.; Li, S.; Li, P. Self-Assembled Amphiphilic Chitosan Nanomicelles to Enhance the Solubility of Quercetin for Efficient Delivery. *Colloids Surf., B* **2019**, *179*, 519−526.
(45) Yildirim, A.; Ozgur, E.; Bayindir, M. Impact of Mesoporous Silica Nanoparticle Surface Functionality on Hemolytic Activity, Thrombogenicity and Non-Specific Protein Adsorption. *J. Mater. Chem. B* **2013**, *1* (14), 1909−1920.
(46) Zha, Z.; Choi, S. R.; Ploessl, K.; Alexoff, D.; Zhao, R.; Zhu, L.; Kung, H. F. Radiolabeling Optimization and Preclinical Evaluation of the New PSMA Imaging Agent [18F] AlF-P16−093. *Bioconjugate Chem.* **2021**, *32* (5), 1017−1026.
(47) Subramanian, S.; Pandey, U.; Morais, M.; Correia, J. D.; Santos, I.; Samuel, G. Comparative Biological Evaluation of Two [99mTc (CO) 3]-Dextran Pyrazolyl Mannose Conjugates Developed for Use in Sentinel Lymph Node Detection. *QJ. Nucl. Med. Mol. Imaging* **2014**, *58* (2), 216−223.

https://doi.org/10.1021/acsomega.4c05991
ACS Omega 2024, 9, 42410−42422